Measurement of n-p and n-d Total Cross Sections from 0.7 to 3.6 GeV/c *

T. J. Devlin, W. Johnson, J. Norem,† and K. Vosburgh‡
Physics Department, Rutgers-The State University, New Brunswick, New Jersey 08903

R. E. Mischke§
Joseph Henry Laboratories, Princeton University, Princeton, New Jersey 08540

W. Schimmerling‖
Princeton-Pennsylvania Accelerator, Princeton, New Jersey 08540

(Received 8 February 1973)

We present direct measurements of the total cross section for neutrons on protons and deuterons in the momentum range 0.7 to 3.6 GeV/c. Using these and other nucleon-nucleon total cross sections, we evaluate total cross sections in the pure isospin states.

I. INTRODUCTION

Measurements of the neutron-proton and neutron-deuteron total cross sections in the momentum range 0.7–3.6 GeV/c are reported here. In an earlier paper[1] we gave a brief discussion of our results. Only a few direct measurements above 0.7 GeV/c exist.[2-5] Our data are the first with both high statistical precision and good momentum resolution in this momentum range. The most extensive previous determination of neutron-proton cross sections at incident momenta greater than 1.1 GeV/c used the cross sections for proton-deuteron and proton-proton scattering to obtain the neutron-proton cross section.[6] In such a calculation a correction must be made to account for the screening effects in the deuteron. Our direct measurements require no such correction.

In the momentum band covered by our data, the np and nd cross sections have the following features. The cross sections decrease sharply with rising neutron momentum at the lower end of our range (0.7–0.9 GeV/c). As the momentum increases, various inelastic processes become possible; the cross sections show minima at ~0.95 GeV/c and begin to rise. The nd cross section rises very sharply to a plateau above 1.8 GeV/c. The slope is slightly negative above ~2.2 GeV/c. The np cross section shows a more gentle rising trend through the momentum band 0.95–2.5 GeV/c, with a prominent bump at ~1.45 GeV/c. It is constant, within uncertainties, from 2.5 to 3.3 GeV/c.

Using our measured np cross sections and measured pp cross sections from several sources,[6-7] we have computed the cross sections for the isotopic spin $I=0$ nucleon-nucleon scattering state. The cross sections for the $I=0$ and $I=1$ states show no convincing indications of resonant effects. The measured nd cross sections have been compared with corresponding previously measured pd data.[6,8] These cross sections are expected to be equal on the basis of charge symmetry, but systematic discrepancies among the data sets are evident. Finally, we compute the neutron-neutron cross section from our measurements, using the deuteron screening correction.[9]

The experiment was performed at the Princeton-Pennsylvania Accelerator (PPA). The momentum of the neutrons was determined using time-of-flight (TOF) techniques and the neutron flux was monitored by several counter telescopes. The attenuation of the neutron beam by hydrogen and deuterium targets was measured with a "good geometry" transmission detector. The total cross section was obtained by extrapolation to zero solid angle, which corresponds to direct forward scattering. Particular care was taken throughout the experiment to measure possible systematic errors which would affect the data. Final corrections to the data for recognized systematic biases were comparable to the statistical uncertainties. The statistical accuracy of the data is between 0.2% and 0.7% for most of the 26 momentum bins, and the total systematic uncertainty is believed to be even less.

II. DESCRIPTION OF THE EXPERIMENT

A. The Beam

The neutral beam was produced at an angle of 20° relative to the proton beam direction (Fig. 1). The protons from the PPA had an energy range of 2.9–3.0 GeV and an average intensity of 4×10^{11} sec^{-1}. Contamination of γ's was reduced by placing 5 cm of Pb 1 m from the synchrotron target. A dipole magnet 9 m from the PPA target swept out charged particles. The primary collimator was 4.445 cm in diameter and was located 22.5 m

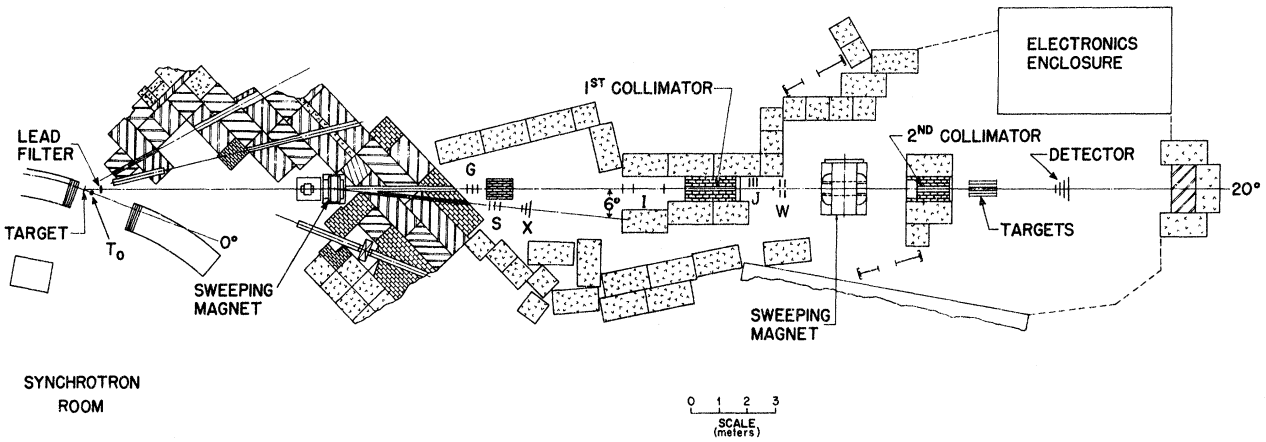

FIG. 1. Plan view of the 20° neutral beam at PPA.

from the PPA target. It was followed by a second sweeping magnet and a secondary collimator, which eliminated charged particles created in the primary collimator.

The beam was mainly composed of neutrons. The neutron flux downstream of the primary collimator was estimated to be 2×10^4 sec^{-1} in the momentum range 0.9–3.6 GeV/c. The flux of neutral K mesons was computed to be 0.15% of the neutron flux. Possible effects of K contamination are discussed in Sec. IV C.

The beam profile (Fig. 2) was measured using a 2.54×0.32-cm^2 counter.

B. The Target System

The target system consisted of three identical flasks surrounded by liquid-H_2 (LH_2) jackets. Their inner diameters were 10 cm and each was 91.5 cm in length. The target flask ends were made of 0.13-mm Mylar, which was covered by four layers of 0.006-mm aluminized Mylar. The outer vacuum flask had windows of 0.25-mm Mylar, so the material in the beam (other than air) was 0.112 g/cm^2 compared with 6.5 g/cm^2 of LH_2 and 15.1 g/cm^2 of liquid D_2 (LD_2). The upstream ends of the targets were located 31.35 m from the PPA target. The target assembly is shown in Fig. 3.

One flask was filled with high-purity LH_2, and a second was filled with high-purity LD_2, while the third was evacuated. Samples of the target contents were assayed for contaminants as discussed in Sec. IV D. The target flasks were sealed to provide stable conditions free of boiling. The LH_2 jackets which surrounded the target flasks were fed from a common LH_2 reservoir.

The three target flasks, denoted H, D, and V (for vacuum), were suspended side by side from a wheel-mounted framework so that each could be moved into the beam. A microswitch-controlled motor-driven mechanism was constructed to move the targets. The detector electronics were coordinated with this system so that the targets could be cycled quickly (typically a full cycle of all targets in 15 min), while the data for the various targets were stored in three separate scalar arrays. This "fast-cycling" feature reduced long-term systematic drifts in the cross-section data. One can view these drifts as manifestations of the

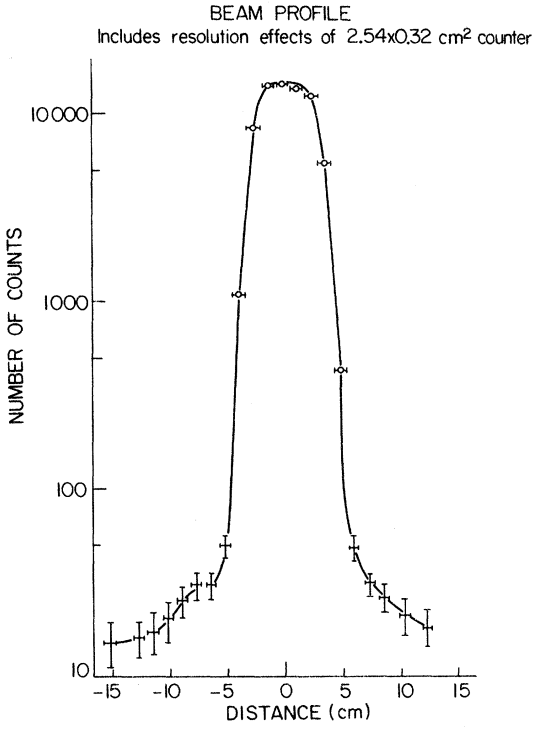

FIG. 2. Measured horizontal profile of the 20° neutral beam.

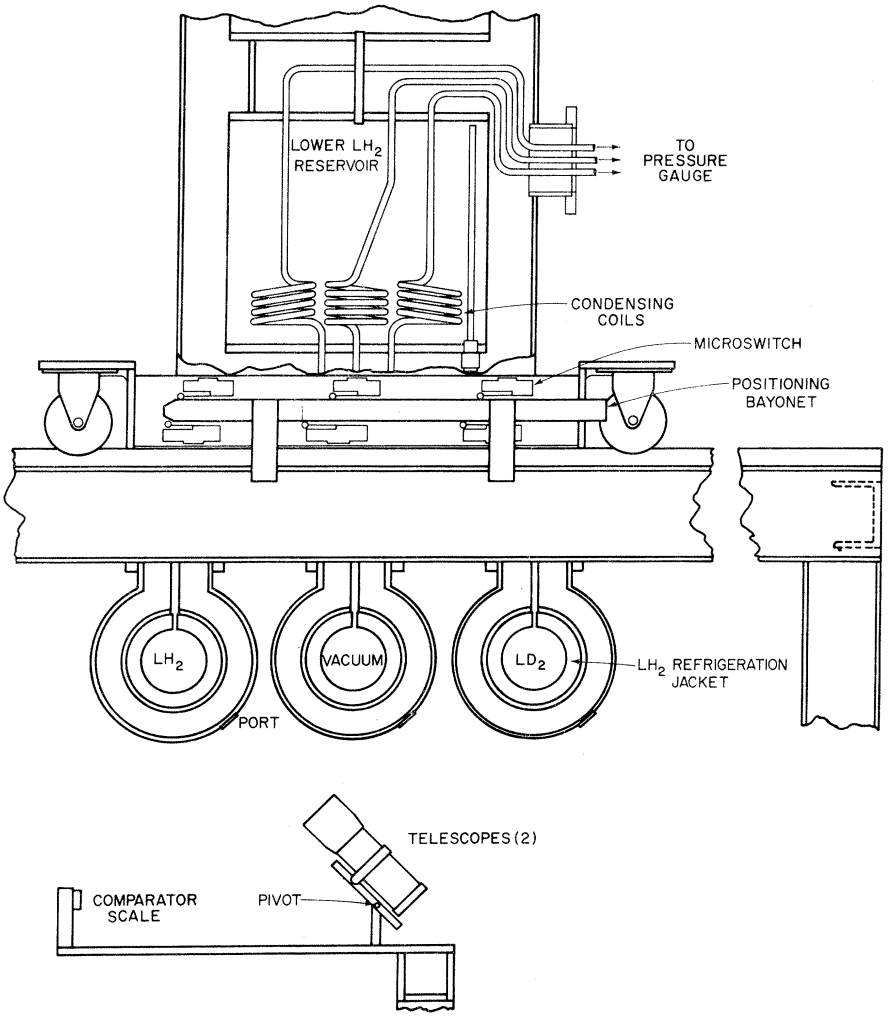

FIG. 3. Drawing showing the major features of the hydrogen-vacuum-deuterium target assembly. In the position shown, the beam passes through the LH_2 target. The two telescopes are rigidly mounted to a common frame which pivots about the axis shown, one viewing each end of the target. The comparator scale and the target ends are the same distance from the pivot to avoid the need to refocus the telescopes. The positioning bayonet was fixed to the stationary frame, while the microswitches were mounted on the moving carriage. Not shown are details such as the cryogenic plumbing and aluminized Mylar insulation.

"$1/f$ noise spectrum" which affects most experiments operating in the frequency range below a few hundred Hz. The rapid cycling has an effect analogous to that of a lock-in amplifier, viz., it raises the operating frequency of the experiment by some factor, N, to a point where the noise amplitude is lower by a factor of N. In our case, N is about 16, i.e., four cycles per hour over a typical four-hour run. If the noise in each cycle is statistically independent, the net improvement is about $N^{1/2}$. If there are positive correlations during a series of cycles, the improvement is even better—up to a factor N.

The axes of the three target flasks were parallel and 27.94 cm apart in the horizontal plane containing the beam axis. The target positions were indicated by a microswitch system mounted on the target frame. The position switches were used to control the target drive system, a DC motor with worm-gear drive. The sensing logic provided a routing signal to control the handling of the data and a gating signal to ensure that no data were collected unless a target was properly aligned. The target positions were measured to be reproducible and aligned on the beam axis within ±2 mm.

The end windows of the targets could be viewed from the side directly through Mylar ports in the vacuum jackets. We made frequent direct measurements of target length. The hydrogen and

deuterium flasks were found to be 914.15 mm and 913.89 mm long, respectively. These figures were reproducible to 0.25 mm.

C. Monitors

The neutron flux was monitored by four scintillation-counter telescopes shown in Fig. 1. Two counter telescopes, G and I, were placed upstream of the primary collimator; a third, J, detected particles scattered from the primary collimator walls; and a fourth, W, counted particles emerging at wide angles from a converter in the beam. In addition, two scintillation-counter telescopes were mounted in the short charged beam created by the first dipole magnet. These were used to calibrate the TOF system, check for beam performance, and measure accidentals due to beam rates.

The redundancy inherent in the large number of monitors allowed the deletion of any monitor which temporarily malfunctioned. The final monitor rates used for normalizing the neutron rate were determined by a fitting process described in Sec. IV B. The resultant normalization factors were compared for different runs; the discrepancies were purely statistical (0.3% for a typical run).

The physical design, position, and electronic resolving times of the monitors were selected to reduce monitor accidental coincidences as much as possible without sacrificing statistical accuracy. Accidentals were measured continuously, and were found to be about 1% for the I monitor, 0.3% for the J monitor, and less for the other neutral beam monitors. Accidentals were subtracted before the data were used.

D. The Neutron Detector

A schematic drawing of the neutron detector is shown in Fig. 4. The scale has been expanded along the beam direction for clarity. The detector was 61×61 cm^2 transverse to the beam and 33 cm thick. The assembly was enclosed in a large aluminum box to minimize electrical noise and environmental changes. The four detection modules were sensitive to neutrons which interacted in 3.8-cm-thick cylindrical conversion volumes 12.70, 20.32, 26.18, and 30.48 cm in diameter. Outside these regions the modules were filled with materials of the same density as the conversion volumes, so that the amount of material encountered by a neutron would be independent of its distance from the beam axis.

Each module consisted of (a) an initial $0.635\times61\times61$-cm^3 veto counter (type 2), (b) a 3.2-cm-thick Lucite conversion volume surrounded by liquid scintillator placed in anticoincidence to define the conversion volume (type 0), (c) a 0.635-cm-thick cylindrical scintillator (type 1) which was part of the conversion volume and served as the first "yes" counter for the charged reaction products, (d) a $0.635\times61\times61$-cm^3 "yes" counter (type 2), and (e) the range telescope. The type-2 "yes" scintillator for each module served as the initial veto for the following module. The neutron TOF was determined by the signal from the cylindrical "yes" scintillator.

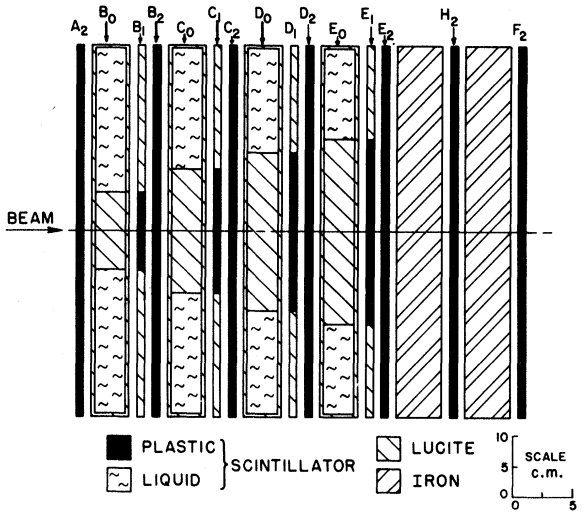

FIG. 4. The neutron detector. The first module consists of a plastic scintillator veto counter (A_2), a cylindrical Lucite conversion volume surrounded by a liquid scintillator veto (B_0), a thin cylindrical plastic scintillator (B_1) embedded in Lucite, and a 61-cm-square plastic scintillator (B_2) in coincidence with B_1. Counter B_2 acts as the initial veto for the next module, and the pattern is repeated through E_2. Finally, the iron-scintillator sandwich, $E_2H_2F_2$, acts as a range telescope for all four modules.

The range telescope consisted of three $0.635\times61\times61$-cm^3 scintillators E_2, F_2, and H_2, with two 3.8-cm-thick iron absorbers sandwiched between. For each accepted event, signals were required from all three range counters. The range cutoff was different for each module because those downstream of the trigger module also contributed to the total range material. This effect was observed as a slight shift in the TOF spectrum cutoff from module to module.

The coincidence combinations which were required for an acceptable module trigger were

$$B=\overline{A}_2\overline{B}_0B_1B_2E_2F_2H_2,$$

$$C=\overline{A}_2\overline{B}_2\overline{C}_0C_1C_2E_2F_2H_2,$$

$$D=\overline{A}_2\overline{C}_2\overline{D}_0D_1D_2E_2F_2H_2,$$

$$E=\overline{A}_2\overline{D}_2\overline{E}_0E_1E_2F_2H_2.$$

The barred signals indicate anticoincidence.

Data were taken with the detector at different distances from the transmission targets. (See Table I.) This procedure increased the range of solid angles subtended by the detector, thus improving the accuracy of the extrapolation to zero solid angle.

E. Data Acquisition System

A schematic representation of the data acquisition system is shown in Fig. 5. Three groups of signals existed: the T_0 counter which gave the neutron production time, the neutron detector which gave the detection time, and the various monitor telescopes. In addition, the target cycling system provided information about which target was in the beam. Data were collected in a 4096-channel pulse-height analyzer (PHA) and in scalers.

The neutron production time was measured by a Čerenkov counter (T_0) mounted near the synchrotron target. The T_0 counter fired every time a bunch of protons struck the synchrotron target. The detector signals were processed by fast electronics. Relative timing of counters in various coincidences were accurate to 1 nsec with pulse widths typically 7 nsec. The monitor telescopes were processed by standard discriminator-coincidence combinations. Six monitor-telescope signals were available for scaling and calibration studies. A master gate incorporating target cycling signals and instrumental dead times was used to gate all detector and monitor logic circuits.

A block diagram of the detector electronics is shown in Fig. 6. The system produced scaling signals for each of the four detector modules and a two-bit signal for module identification. A third bit was set whenever two detector signals arrived within 150 nsec of each other (multiple module events).

A signal from any one of the modules resulted in START and STOP signals for a time-to-amplitude converter (TAC). The relative timing of various signals in the detector coincidences was arranged so that the final output coincidence pulse (STOP) had a leading edge determined by the type-1 scintillator in the appropriate module. The STOP signal was also used to generate a pulse with a width equal to the proton bunch spacing in the synchrotron (67.3 or 134.6 nsec) which acted as a gate to select the most recent signal in the T_0 pulse train (Sec. III A) for production time. A second level of gating was added to avoid leading-edge ambiguities in the production of the START signal.

Appropriate delays in the individual module electronics were made to ensure that neutrons of the same momentum converting in different modules used the same operating range of the TAC and the analog-to-digital converter (ADC).

The ADC provided eight bits of the 12-bit address in the PHA. The other four bits were derived from the module and target identification bits. Thus, the 4096 channels of the PHA were separated into sixteen 256-channel "banks." Twelve of these banks were used to store the TOF information in the events from four modules for each of three targets. Three more were used to store TOF spectra from multiple module events.

Signals other than a neutron detection event could be selected as input for the TOF logic. During calibration runs, TOF spectra were obtained for the various monitors and for the signals

TABLE I. Detector parameters.

Detector position	Module	L_0[a] (m)	t_γ (nsec)	L_1[b] (m)	$\Delta\Omega$ (raw) (msr)	$\Delta\Omega$ (corr.) (msr)
1	*B*	34.50	115.0	2.703	1.73	1.56
	C	34.56	115.2	2.762	4.25	3.97
	D	34.62	115.4	2.824	6.76	6.32
	E	34.68	115.6	2.884	8.74	8.37
2	*B*	35.98	119.9	4.185	0.72	0.64
	C	36.04	120.1	4.244	1.80	1.67
	D	36.11	120.4	4.306	2.91	2.70
	E	36.17	120.6	4.366	3.82	3.63
3	*B*	37.50	125.0	5.701	0.39	0.35
	C	37.56	125.2	5.760	0.98	0.90
	D	37.62	125.4	5.822	1.59	1.48
	E	37.68	125.5	5.882	2.11	2.00

[a] Distance from source to detector.
[b] Distance from target center to detector.

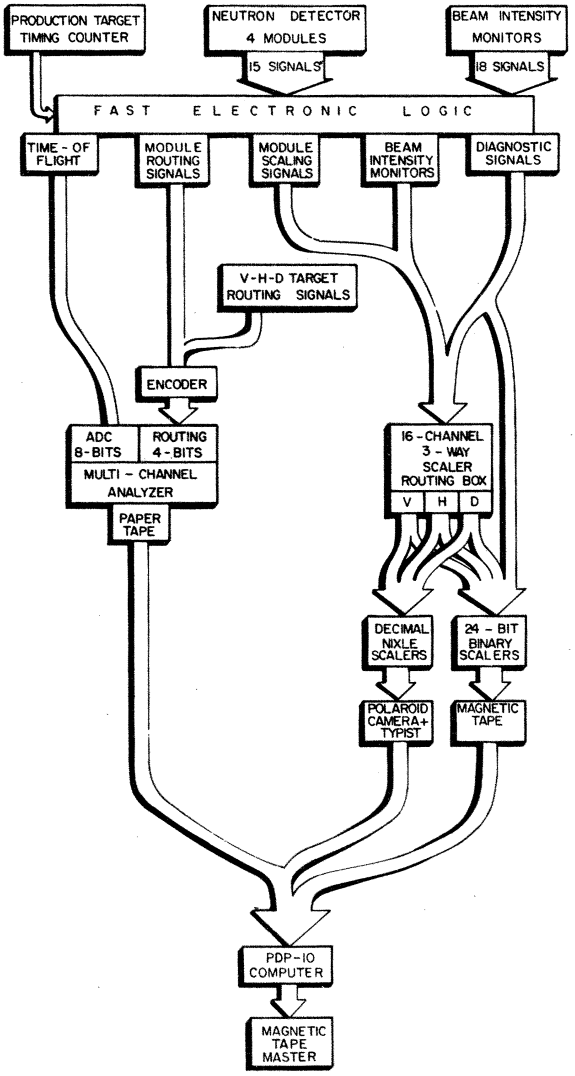

FIG. 5. A schematic representation of the data acquisition system.

from a pulse generator.

We used 100-MHz 7-digit Nixie decimal scalers and 20-MHz 24-bit blind binary scalers to record counters from the various monitors and detector modules. Three scalers were devoted to each of the signals in order to accumulate separately the data from the V, H, and D phases of the target cycling procedure. A series of 20-MHz AND gates were used to route the scaler signals to the appropriate units. These gates were enabled by levels generated in the target cycling system.

Some diagnostic signals, e.g., those used to check gain drifts in the counters (See Sec. III B), were scaled only for the vacuum target or were summed for all targets.

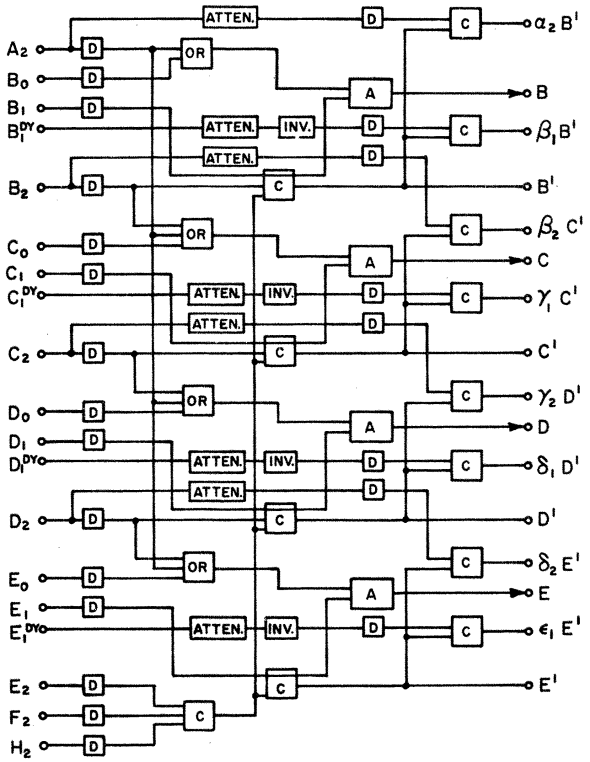

FIG. 6. A block diagram of the detector electronics. Key: D — fixed threshold discriminator; C — coincidence; A — anticoincidence; ATTEN — attenuator; INV — inverter; —○ — scalar output; →○ — further connection with electronics not shown.

III. EXPERIMENTAL PROCEDURES

A. Measurement of Neutron Momentum

The momentum of each detected neutron was determined from the neutron's TOF. This method was used in a number of experiments at the PPA.[10-14] Figure 7 shows a TOF spectrum. Typically the time resolution was 1.7 nsec full width at half maximum (FWHM), giving $\Delta P/P = 1.1\%$ at $P = 0.7$ GeV/c and $\Delta P/P = 13.3\%$ at $P = 3.0$ GeV/c.

Since proton bunches struck the synchrotron target every 67 nsec, there was an ambiguity in the TOF. It was impossible to tell from TOF alone which proton bunch created a given neutron. This difficulty was solved by inserting steel range material in the detector to provide a threshold in detected momentum. The steel thickness was chosen to give the fullest usable spectrum of momenta, without contaminating the high-momentum-data with low-momentum "ghosts"[11] from the previous proton bunch.

B. Calibration and Checking Procedures

There are several effects that could result in systematic errors in the cross-section measure-

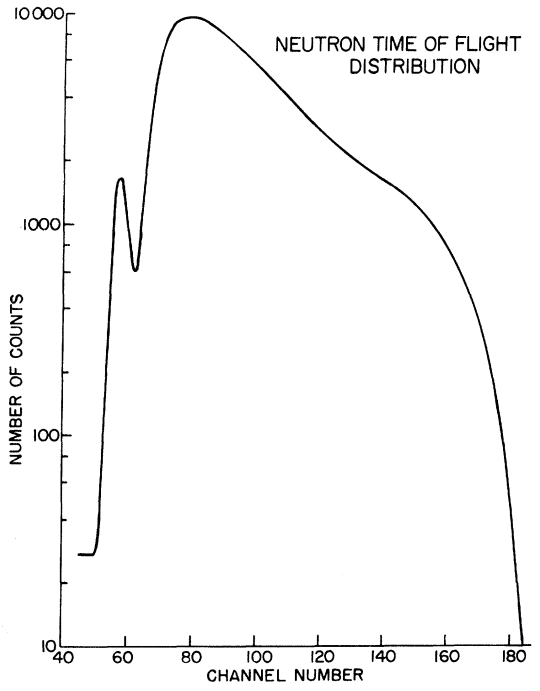

FIG. 7. Neutron time-of-flight distribution. For this particular run the conversion factor is 0.4808 nsec/channel. The small peak at left is due to γ's. These data were taken for the B module during a doubly chopped run.

ment. Some of these are (1) variations in the detector efficiency, (2) inaccurate determination of the PHA time scale and origin, drifts in timing, or lack of linearity in the TOF system, (3) beam contamination due to protons in the supposedly empty synchrotron phase-stable regions (alternate bunch contamination) which would not satisfy the momentum discrimination requirement, and (4) variations in the beam spill quality. Possible systematic errors due to these effects will be discussed in Sec. IV. In order to provide a diagnostic for possible malfunctions occurring during the run, and to ensure proper calibration of the apparatus, the following procedures were used.

1. The detector efficiency can vary due to photomultiplier gain changes and due to mechanical deformations in the scintillator and light-pipe assemblies. Temperature changes will cause variations in the behavior of the electronic components which appear as changes in efficiency; they may also be the source of mechanical stresses.

The temperature of the electronics enclosure was kept constant using air conditioning and fans on the electronic racks. Air from this enclosure was blown through a hose to the detector box in order to keep it at a constant temperature also.

Every photomultiplier was operated well into its voltage plateau in order to have minimum dependence on drifts in the high voltage and to have high efficiency. All voltages were recorded frequently throughout the experiment and observed changes were smaller than 0.1%.

Auxiliary signals were derived from the type 1 and 2 counters to monitor the counter efficiency. These signals were attenuated and placed in coincidence with the normal type 1 and 2 signals from each module together with the F_2 signal. The attenuation was chosen to correspond to the 50% point on the voltage plateau for maximum sensitivity to changes in photomultiplier gain. In addition, the relative counting rates for each of the four modules were recorded and compared. Some discontinuous changes in the relative efficiencies were found, mainly in the efficiency of E, the largest of the detector modules. These changes could not be traced to any single cause. They may have been due to occasional temperature variations which are known to have occurred. Data runs showing such an abrupt variation in efficiency are excluded from the analysis.

2. The proper functioning of the TAC as well as the linearity of the TOF system were checked by using a pulse generator as the event signal. Since there is no correlation between the pulses from the generator and T_0 pulses, a uniform distribution of time intervals, or "white spectrum," resulted. Nonlinearities in the analyzer found in this way amounted to less than 0.5%.

Drifts in T_0 timing were monitored using a "time vernier." To set up this system, the S monitor signal was placed into a delay coincidence with T_0. Two coincidence circuits were used with delays chosen to make the S signal arrive at the 50% points of the rising and falling portions of the relative delay curve. The output from each coincidence was scaled and the ratio of counting rates determined timing shifts. The system is sensitive to shifts of approximately 0.1 nsec. The S monitor was used since it detected relativistic charged particles with a TOF peak of 1.5 nsec FWHM and background <0.1%.

3. The S monitor was also used to monitor the alternate bunch contamination.[11,13] To do this, an ST_0 coincidence was set up and compared with the same coincidence obtained by delaying T_0 by 33 nsec. The alternate bunch contamination was of order 0.1% or less for all the data retained for analysis.

4. The momentum of the proton beam varies due to the sinusoidal time variation of the synchrotron magnetic field. In addition, synchrotron oscillations result in a secondary-beam intensity that is not uniform throughout the proton targeting (spill) time. The master gate enabled the fast

logic only during a predetermined interval within the spill time, near the peak proton momentum. This interval was chosen to obtain uniform beam intensity; it corresponds to proton momenta between 3.70 and 3.85 GeV/c.

Variations in the spill rate as a function of spill time within this interval, and thus, as a function of proton momentum, were monitored using the X telescope. The X monitor counts were separated into four spill-time regions and recorded separately on four scalers for each target using timing signals from the synchrotron to gate a signal correlator. The four relative counting rates were always target-independent within the uncertainties of counting statistics.

C. Tests and Preliminary Runs

Many of the tests and preliminary runs were designed to detect suspected malfunctions of the apparatus or physical processes which could affect the cross sections. These will be listed below, together with the conclusions which were reached.

1. A run was taken with 122 cm of Pb in the neutron beam. The event rate was reduced by a factor of 5×10^{-5}, which indicates that there is no significant source of events other than beam induced events. In fact, the event rate was consistent with that expected from cosmic rays.

2. Runs were made with additional shielding before the primary or secondary collimator. These runs were tested for leakage around the collimators and none was found.

3. The routing signals were reversed to interchange PHA banks for target-full and target-empty data. If there were problems related to the routing system or PHA banks, the cross sections could be affected. No effect was seen.

4. Several runs were recorded to check for possible rate dependence of the cross sections. One run was taken with the accelerator beam at $\frac{1}{2}$ intensity. Other runs were made with beam intensity reduced by partially closing the beam jaws. These runs indicated that there were no major problems with accidentals.

5. Tests were made to check the effects of possible beam contaminants. Runs were taken with additional Pb in the beam and with 45 cm of CH in the beam to change the beam composition. A run was taken with the Pt production target replaced by a Be target. Again the cross section showed no effect.

6. Runs were taken with the V flask filled with LH_2 and with all three flasks evacuated. These gave zero "cross sections" within errors, as expected.

7. A 1.9-cm-thick Al plate was inserted just downstream of the target flasks. The sheet contained a 10.8-cm-diameter hole centered on the beam line. The intention was to enhance any effects due to interactions in the target structure by particles scattered from the LH_2 or LD_2 and particles in the beam halo. No effect was observed from this test.

8. Several runs were taken with doubly-chopped injection and with the singly-chopped range requirement to study ghost contamination. If the range requirement were successful, one would expect the second half of the 134-nsec TOF spectrum to be empty. The observed rate was consistent with accidentals. We conclude that ghosts were eliminated.

D. Data Collection Procedures

The rapid-cycling feature of the target system allowed "simultaneous" data taking for H and D with a common V in between. The dwell times were set to give one half as much beam through the D target as through the H and V flasks on each cycle. This matched the statistical precision since the attenuation for D was approximately twice as much as that for H.

At the end of each data run (four to eight hours), the PHA data were punched onto paper tape; the binary scaler data were written on magnetic tape, and the Nixie scalers were photographed. These data were merged onto a single magnetic tape for off-line analysis. The Nixie scaler data were proofread after typing in order to check for errors. Various scaler ratios were computed and plotted as functions of run number in order to search for drifts, instrument failures, and typographical errors. Further error searches were made with higher-level statistical comparisons during the cross section calculations. The raw data tape was edited several times when data transmission errors (usually a single bit) were discovered.

Following each data run the Pb filter was removed and a short run was taken to check the location of the TOF peak due to γ's. Data were taken with two different cable lengths before the TAC giving two peak locations. These were used to establish the time origin and time scale in the PHA.

Particular attention was devoted to the problem of making accurate measurements of the target density. The target pressures were measured every two hours using a precision pressure gauge calibrated by the manufacturer against a standard from the National Bureau of Standards. The pressure measurements were accurate to 2 g/cm^2, which corresponds to estimated density uncertain-

ties of 0.04% for LH_2 and 0.06% for LD_2. In part, our concern was prompted by unexplained differences[15] of ~0.5 °K between the calculated temperatures of the LH_2 jackets and LD_2 flasks in two previous experiments.[6,8] A similar effect, ~0.3 °K, occurred during the initial operation of our target in another experiment.[10] To ensure that the target pressure was measured under well-defined thermal conditions, the liquid-vapor interface was kept inside the target flask. The temperature in this region was determined by the LH_2 jacket, and was not affected by any temperature gradients along the filling tubes. The temperatures at the liquid-gas interface were computed from the measured pressures using the tables of Tapper.[16] Under the conditions described, the LH_2 and LD_2 temperatures were found to agree within 0.1 °K.

The data collected for the cross sections can be grouped into four distinct sets. The first, consisting of 10^8 events, was not used because of a design flaw in a commercial TAC. The defective unit was replaced for the remainder of the experiment. The data in the first set were useful only for diagnostic purposes. The remaining sets were all used in calculating the final cross sections. The second set, referred to as the "old" data, consisted of 1.2×10^8 events. About halfway through the data collection period, two major changes were made in the electronics in order to reduce accidentals. Up to that time the accidentals rates required corrections to the cross sections ranging from about 1% for the B module to about 3% for the E module. Our experience with the detector to that time showed that gain and timing drifts were quite small over periods of several days, and that the rapid cycling of the targets reduced the effects of such drifts to negligible importance. Therefore, we decided to reduce the pulse widths used in the detector coincidence circuits, and to reduce the voltages on the photomultipliers for the type-1 counters from typically 400 V above the knee of the plateau curve to about 200 V above the knee. The first reduced accidentals from all sources, and the second reduced those resulting from noise probably unrelated to beam intensity. Further reduction in accidentals was achieved by decreasing the beam size from 7.6 to 6.3 cm in diameter. After these changes we took a third data set, 1.3×10^8 events, which is referred to as the "new" data. Finally, we took 0.4×10^8 events with doubly-chopped injection to extend the sensitive range of incident neutron momenta down to 0.7 GeV/c.

Data were taken to measure the effective solid angle of the detector. This was done by moving the entire detector array with respect to the neutron beam. The data were analyzed, taking into account the known beam profile (Fig. 2), and the results have been used in Sec. IV E.

E. Detector Accidentals

Although the rate of detected neutrons was of order 400/sec, the total number of neutrons in the beam of all momenta may have been about 10^5/sec. About 10% of these probably interacted in our detector without fulfilling the requirements for a valid neutron signal. Thus, we observed singles rates in some elements of our detector in excess of 10^4/sec. This gave rise to a small, but significant rate of accidental neutron triggers. The logic contained a requirement of five "yes" counters and the absence of two veto counters for each valid count. The accidental contribution was different for each module, for each portion of TOF, and as a function of target full and empty.

In order to get a valid measurement of the accidentals, it was necessary to perform a series of measurements with logical requirements which counted all possible combinations of two particles which could simulate a trigger (but excluding coincidences between two valid events). The technique used was to select one particle, which satisfied only part of the logic, and then form the rest of the coincidence with a different particle which arrived 67 nsec later. Care was taken to preserve the widths and relative timing (module 67 nsec) of all signals involved.

Accidental coincidences between yes counters gave a number of counts to be subtracted while accidental vetoes indicated counts to be added. The two terms tended to cancel, making the net correction small. The correction was largest for the E module for three reasons. First, it was the last of the four modules, and detected particles produced in the other three. Second, the E module had only four coincidence counters (since E_2 was the fifth counter for other modules), and thus the electronics requirement was not as strict. Third, the E module was the most compact longitudinally, so there was a larger solid angle for particles scattered in it.

We considered only types of accidentals which could be caused by two particles. For example, the full logical requirement for triggering the C module of the detector was $\overline{A}_2\overline{B}_2\overline{C}_0C_1C_2E_2F_2H_2$. One type of accidental might consist of a short-range charged reaction product, which converted in the correct interaction volume but stopped in the steel after E_2, along with another beam neutron which simultaneously converted in front of F_2, giving the remaining pulses required by the electronics logic. Four two-particle accidentals can be defined for each module (three for the E

module). In addition, each module can be accidentally vetoed.

It was not possible to measure all 19 types of accidentals continuously throughout the experiment. We adopted the assumption that all types of accidentals including those in the monitors would be proportional to beam rate, and therefore to each other. Several were selected for continuous monitoring. The others were measured to determine a set of ratios once during each of the two major data-collection periods. Run-by-run corrections were made on the basis of the accidentals ratios and the rates for selected types measured during each run. Our assumption that the accidentals ratios would remain constant was not completely borne out by the data. Nonstatistical fluctuations up to 20% were observed. The greatest uncertainty in the accidentals correction was due to the lack of a monitor which gave a reliable measure of the variation of the accidentals rates from run to run. The corrections to the cross sections after the changes were less than 1% for all modules. The data for the two periods were analyzed separately as described in Sec. IV E.

IV. DATA ANALYSIS

A. Time of Flight

In our TOF system the quantity directly measured is $(t - t_\gamma)$, where t and t_γ are the flight times for neutrons and γ's. We use the relation

$$t - t_\gamma = k(C - C_\gamma), \tag{4.1}$$

where C_γ = channel number for the center of the γ peak, C = channel number for the neutron event, and k = conversion factor from channels to nsec. The value of t_γ was computed from the various source-to-detector distances and was different for each module because of longitudinal displacements. (See Table I.) Differential and integral nonlinearities in the TOF system were absent at a level better than 1%. Therefore, we made no nonlinear corrections to Eq. (4.1). C_γ was different for each module, but k was common to all and had a value typically 0.4824 ± 0.0008 nsec/channel. The values of C_γ and k were measured for each run. The quoted uncertainty in k combines measurement uncertainties and drifts during single runs.

We chose momentum-bin boundaries corresponding to the momentum values given in the data tables of Sec. V. The bin widths were always consistent with the TOF resolution of 1.7 nsec. Rarely did the boundary between two momentum bins fall exactly on the boundary between two TOF channels. Counts in the TOF channels on a bin boundary were split between bins in proportion to the amounts of overlap, with a correction for the variation of the TOF spectrum across such a channel.

Although drifts in the TOF electronics had negligible effect on the momentum determination, it is necessary to consider how such drifts can affect the cross section measurement. If the TOF spectrum were flat, a shift in the calibration parameters C_γ and k between vacuum and hydrogen targets would have no effect on the apparent cross section. However, the spectrum was not flat. An undetected timing shift between the two target exposures can be misinterpreted as a change in attenuation in direct proportion to the slope of the spectrum in any TOF channel.

It is important to emphasize that only true drifts in the TOF electronics contribute to this effect. Simple calibration errors apply equally to all targets and contribute only to errors in the momentum used to label the cross section. The most serious drift is one which is correlated with the target selected; the effects of all other types tend toward zero because of target cycling.

By direct observation during the experiment, we established that the dependence of C_γ on beam rate was, at most, a small fraction of a channel width. However, after a large number of runs had been collected and computer evaluation of C_γ and k performed, we found a small, but well-defined rate dependence in these parameters. The effect was of order 0.3% over the range of variation encountered. With this information, we were able to compute corrected values of C_γ and k for the true rates encountered in the V, H, and D target exposures.

The effect was serious for deuterium in the momentum bins above 2.3 GeV/c. E.g., at 2.944 GeV/c the shift in a typical run between V and D exposures was (15 ± 5) picoseconds and resulted in a change in cross section of (-1.37 ± 0.46) mb for deuterium compared with a calculation neglecting this shift. The quoted uncertainties in the highest momentum bins are dominated by this effect. Below 2.3 GeV/c, the change was less than the statistical uncertainties on the points. The corrections and uncertainties for hydrogen are lower by roughly half.

After the dependence of k on beam rate was taken into account, there remained no observable drifts in the calibration parameters. We can put an upper limit of 0.05 mb on uncertainties in the cross section due to any such residual effects.

B. Beam Monitors

When possible, we used the sum of all four neutral beam monitor telescopes (corrected for ac-

cidentals) as a relative measure of the neutron flux during each of the three target exposures. We define

$$M_i \equiv G_i + J_i + W_i + I_i \equiv \sum_j m_{ij} , \quad (4.2)$$

and use subscript $i = 1$, 2, and 3 to refer to V, H, and D targets, respectively, and subscript $j = 1$, 2, 3, and 4 for the monitors G, J, W, and I, respectively.

Any variation (outside statistics) of the relative contribution of individual monitors to M_i is a measure of the monitor inconsistencies from target to target. Under ideal conditions

$$m_{ij} \simeq f_j M_i \quad (4.3)$$

within statistical fluctuations, where f_j is the fractional contribution of the jth monitor to M_i, and f_j is independent of target. We formed a statistical test of this hypothesis,

$$\chi^2 = \sum_{i,j} (m_{ij} - f_j M_i)^2 / m_{ij} , \quad (4.4)$$

and varied f_j and M_i to produce a minimum in χ^2 subject to the constraint

$$\sum_j f_j = 1 . \quad (4.5)$$

The fit has twelve pieces of data, seven parameters, and one constraint, yielding six degrees of freedom (DF = 6).

For most of the 62 data runs and 10 accidental runs, the values of χ^2 were acceptable. Six runs had χ^2 probabilities $P(\chi^2) < 0.01$. We improved the fit by discarding the monitor with the highest contribution to χ^2. Early runs were taken before the W monitor was installed, and were analyzed without it. In all, 54 runs had four monitors (DF = 6), sixteen had three (DF = 4), and 2 runs had only two monitors (DF = 2). $P(\chi^2)$ for the 72 runs was histogrammed, and the resultant distribution was essentially flat. We regard this as evidence that our monitor normalization, a crucial part of the cross section measurement, is free of significant systematic error, and that it is a reliable measure of relative beam intensity. Comparison of this work with our earlier experience[10,14] makes it clear that the use of rapid target cycling is chiefly responsible for this situation.

The monitor analysis results in a set of numbers, M_i, $i = 1, 2, 3$, which gives the relative beam flux for the three targets. Uncertainties in M_i (0.14% for a typical run) and very small correlations among them were given by the error matrix from the fitting procedure. This matrix was used in subsequent analysis of the cross sections.

C. Beam Contaminants

Among the sources of systematic error to be considered is the possibility of beam contaminants. These could be either particles other than neutrons, or neutrons of various origins with the wrong momentum for a given TOF bin. We find no significant effect due to beam contaminants. Each of the possibilities is discussed below.

1. γ Rays

The two momentum bins above 2.8 GeV/c are the most likely to be contaminated by γ's from the synchrotron target. The bin boundary at 3.2 GeV/c is slightly over 5 nsec in TOF from the center of the peak of the γ TOF distribution. By removing the Pb in the beam, we measured this shape out to 3.5 nsec directly. Assuming it to be symmetric, we extended this to about 4.5 nsec. The falloff appeared exponential, and we extrapolated it through these two bins. The contamination estimated in this manner was 0.6% of the neutron flux at 3.277 GeV/c, and less than 0.03% at lower momenta. We have neglected it.

2. K_L^0 Mesons

We estimated the K_L^0 flux in our beam from the K^+ production data of Ref. 17, and corrected it for decays in flight to the detector position. The contamination varied between 0.1% and 0.2% of the neutron rate in the various TOF bins. The magnitude of the correction must be weighted by the differences between the K_L^0 and neutron cross sections on our targets. The K_L^0 cross sections can be estimated from the corresponding published K^+ and K^- values.[18] If the detector efficiency for K_L^0 is the same as for neutrons, the correction might be as high as +0.07 mb for deuterium and +0.03 mb for hydrogen. However, we can argue that the detector efficiency for K_L^0 is substantially reduced. The cross sections are lower, and the energies available to satisfy the range requirement are lower by a factor of 2. We neglect this correction and assign a systematic uncertainty of 0.05 mb for deuterium and 0.02 mb for hydrogen to account for it.

3. Secondary Beam Interaction Products

We can estimate the flux of beam-collimator or beam-air interaction products from the magnitude of the beam halo. (See Fig. 2.) The flux amounted

to about 0.15% of the central neutron flux. With areas taken into account, this was between 0.5% and 1% of the total rate. Forward diffraction scattering probably accounted for more than 90% of the events in the small angular range subtended by the second collimator.[14] The neutrons, however, had the same energy, TOF, and cross section as the particles which produced them. Therefore, no correction is required. The remaining particles (<0.1%) were most likely inelastically scattered neutrons and γ's from π^0 decay. From considerations of cross section differences, rates, and detector sensitivity, it is very unlikely that this requires corrections to the cross sections greater than 0.02 mb. Therefore, we neglect it.

4. *Charged Particles*

It is difficult to make direct measurements of any residual charged-particle flux at the end of a neutral beam. The rates observed in scintillation counters placed in our beam were consistent with neutron interactions in the counters, i.e., no charged particles.

We can advance indirect arguments that the charged-particle flux is negligibly small. The final sweeping magnet had ~10 kG m of bending power. No charged particle originating anywhere upstream of it along our beam line could get through the second collimator. Any charged particles resulting from interactions along the rest of the beam constitute part of the halo discussed in the previous section. We assume no separate systematic uncertainty for this effect.

An entirely different aspect of charged particle background arose from a consideration of charged particles resulting from neutron interactions in the target. Such particles affect our results only through inefficiencies in the A_2 veto counter, and then only in the data from the B module. No statistically significant discrepancy between the B-module results and those of the other three modules was observed. The most serious source of charged particles originating from the target was forward elastic charge-exchange scattering. If we assume this equal in magnitude to ordinary forward scattering, then the effect will be reduced from the ordinary forward scattering correction by the inefficiency in A_2. The forward scattering correction was at most of order 1 mb, and usually much lower. The A_2 inefficiency was less than 1%. We conclude that the effect is negligible.

5. *Ghosts*

In Sec. III C, we described the data collected to study "ghost" neutrons which might have succeeded in passing our range requirement. The observed rate was completely consistent with our known accidentals rate. We conclude that ghosts constitute less than 0.1% of the rate of detected neutrons. Since their cross sections are always within 50% of those of the neutrons under study, we assign a systematic uncertainty of 0.05% for this effect.

D. Target Parameters

Measurements of the densities and thicknesses of the hydrogen and deuterium targets were discussed in Sec. II B. Target vapor pressures, temperatures, and densities tended to vary in a manner fully accounted for by changes in barometric pressure. Since a typical data run lasted four to eight hours, several sets of target pressure measurements, taken at two-hour intervals, were averaged to obtain the values used. A typical set of target parameters is given in Table II. The dominant error comes from uncertainties in the tabulated values of molar volumes.[16] The number of interest in computing the cross section is

$$1/nx = V/(2N_0 x), \tag{4.6}$$

where $N_0 = 6.02217 \times 10^{23}$ molecules/mole, V is the molar volume in cm^3, and n is the density in nuclei/cm^3. The effective length, x, has been revised downward by 5.06 mm from the values of Sec. II B to account for curvature of the Mylar windows over the area of the neutron beam.

TABLE II. Typical parameters of hydrogen and deuterium targets.

Parameter	Hydrogen		Deuterium	
Pressure (PSIA)	15.40	±0.02	4.97	±0.02
Pressure (Torr)	797.0	±1.0	275.0	±1.0
Temperature (°K)	20.43	±0.04	20.37	±0.11
Molar volume (cm^3)	28.553	±0.002	23.781	±0.003
Density (g/cm^3)	0.070 603	±0.000 005	0.169 387	±0.000 002
Measurement uncertainty		±0.016%		±0.013%
Table uncertainty		±0.03%		±0.1%
Effective length (cm)	90.91	±0.03	90.88	±0.03
$1/nx$ (mb)	260.8	±0.1	217.3	±0.2

Corrections for HD contamination of D_2 were made according to the procedure suggested in Ref. 16. Analysis of the gas above the LD_2 showed 1.1%, 1.4%, and 1.8% HD by volume for the three times the target was filled. In the case of 1.4%, the cross section for D_2 was revised upward by 0.3%, or about 0.25 mb. This varied somewhat with neutron momentum. If we accept the differences among the three gas samples as characteristic of the uncertainty in this correction, the resultant systematic uncertainty in the n-d cross section is less than 0.1%.

E. Calculation of Cross Sections

1. *General Discussion*

In presenting the calculation of cross sections, we give the characteristics of the data set, the monitor normalization, accidentals corrections, and sources of statistical uncertainties. The last are of particular importance because of correlations which exist among various subsets of the data.

The three types of data, old, new, and "doubly chopped," were subdivided into sets of runs taken at the same detector position (solid angle range). Initially, runs varying between 10^6 and 10^7 events per run were selected for the cross section measurements. Eight of these (3.8×10^7 events) were discarded because of various unsatisfactory running conditions, e.g., more than 0.1% of the synchrotron beam within the supposedly "empty" phase-stable bunches. Another three runs (1.4×10^7 events) were discarded during the cross section analysis when they were found to be inconsistent with others of the same type. There remained 62 runs with over 3×10^8 events. The final cut, about 7%, was for momentum 0.7–3.6 GeV/c for doubly-chopped runs, and 0.9–3.6 GeV/c for the others.

A complete set of five accidentals runs was taken for each of the old and new conditions. The doubly-chopped data were taken under the same conditions as the new data and were corrected accordingly. The division of runs and events among various types is shown in Table III.

The analysis procedure began with computing the cross sections, properly normalized and corrected for accidentals, for each solid angle Ω, in each momentum bin P, in each data run r, and type t. These 11 168 cross sections, $\sigma_{tr}(\Omega, P)$, were then combined into 1296 weighted averages, $\sigma_t(\Omega, P)$, for the various momentum bins and solid angles. Individual deviations from the weighted averages were examined for systematic effects. The three discarded runs mentioned above were identified at this level of analysis. Next, extrapolations to zero solid angle were made, yielding 140 measurements of total cross sections, $\sigma_t(P)$. Finally, old, new, and doubly chopped data were combined to yield the 52 cross sections in our final data set, $\sigma(P)$.

TABLE III. Distribution of data among various types of runs.

	Detector position	Number of runs	Events after cuts
Old	1	11	70 605 124
	2	12	60 044 073
	3	0	0
New	1	4	14 384 205
	2	12	52 123 962
	3	15	67 209 356
Doubly chopped	1	0	0
	2	2	8 713 023
	3	6	27 371 095
Total		62	300 450 838
Old accidentals	1	5	41 821
New accidentals	1 and 3	5	15 036

The old runs were statistically independent of the new and doubly chopped runs. Only a small correlation between new and doubly chopped runs existed because of the very small accidentals correction. Therefore, the three major run types were treated as being statistically independent.

For a given type, the same accidentals runs were used to correct runs at all three positions. This correction was correlated for a given module and momentum bin in all runs at all three detector positions. It did not give rise to correlations between momentum bins or between modules. On the other hand, the monitor normalization gives rise to a correlation between modules and momentum bins within a given run. Thus, it was necessary to keep track separately of the uncertainties in the cross sections arising from counting statistics in the detector, the monitors, and the accidentals corrections. Only the appropriate combinations, in quadrature, were used in the various stages of the analysis. In the extrapolation to zero solid angle, it was necessary to construct a full input data error matrix which expressed correlations among different positions of the same module, and different modules at the same position. The procedure is described in more detail below.

2. *Accidentals Corrections*

We computed the neutron-proton cross section for a given module in a given momentum bin for a given run according to the equation

$$\sigma_{\rm tr}(\Omega, P)_H = (1/nx)_H \ln \frac{(N_V - A_V)/M_V}{(N_H - A_H)/M_H} \ , \qquad (4.7)$$

where $(1/nx)_H$ represents the target parameters [Eq. (4.6)], N is the number of detected neutrons in a module, A is the net number of accidentals in that module (explained below), and M is the corresponding number of monitor counts. The subscripts V and H refer to vacuum and hydrogen targets. A similar equation holds for the deuterium cross sections, and the H (or D) subscript will be omitted from here on.

The five different types of accidentals were measured in five different runs, adjusted to a common accidentals rate in the J monitor, and normalized to 100 000 counts in the G monitor. G was selected for over-all normalization because it had small long term drifts (~3%) and very small accidentals rates. J was selected as a standard for accidentals ratios because of its significant accidentals rates (0.3%) and modest stability (~10%) over long periods.

The net accidentals *rate* for each momentum bin and module was scaled according to the J-monitor accidentals rate in each data run. Then the net *number* of accidentals was computed on the basis of the total number of G-monitor counts for the run. Statistical uncertainties in the accidentals corrections were computed in a straightforward manner. Since the veto accidentals were relatively large, the net correction was often smaller than its statistical error, particularly in the new runs.

3. *Averaging Runs*

Up to 15 runs of the same type were averaged to get the best estimate of the cross sections taken under any given set of conditions. (See Table III.) Cross sections were weighted according to combined detector and monitor variances, i.e.,

$$\sigma_t(\Omega, P) = \frac{[\sum_r w_{\rm tr}(\Omega, P)\sigma_{\rm tr}(\Omega, P)]}{W_t(\Omega, P)} \ , \qquad (4.8)$$

where

$$1/w_{\rm tr}(\Omega, P) = V^m_{\rm tr} + V^d_{\rm tr}(\Omega, P),$$
$$W_t(\Omega, P) = \sum_r w_{\rm tr}(\Omega, P). \qquad (4.9)$$

V^d, V^m, and V^a (below) are the variances for the detector, monitors, and accidentals. For them and for the weights, w, we adopt the subscript and argument notation defined earlier for the cross sections. In order to compute the variances for the average cross sections, we used the average fraction, u, of the total variance due to the monitors. Thus

$$u_t(\Omega, P) = \frac{[\sum_r w^2_{\rm tr}(\Omega, P)V^m_{\rm tr}]}{W_t(\Omega, P)} \ , \qquad (4.10)$$

$$V^m_t = \frac{u_t(\Omega, P)}{W_t(\Omega, P)} \ , \qquad (4.11)$$

$$V^d_t(\Omega, P) = \frac{[1 - u_t(\Omega, P)]}{W_t(\Omega, P)} \ . \qquad (4.12)$$

Although the accidentals correction fluctuated by as much as 50%, it was fully correlated from run-to run and, therefore, was not included in the calculation of the weights. We assume that the variance in the average cross section due to accidentals is simply the average of the individual run variances, i.e.,

$$V^a_t(\Omega, P) = \frac{1}{N} \sum_{r=1}^{N} V^a_{\rm tr}(\Omega, P), \qquad (4.13)$$

where N is the number of runs being averaged.

4. *Solid Angle Corrections*

Because of the finite size of the detectors and beam dimensions, the cross section defined in Eq. (4.7) is not the total cross section. Thus, for a detector subtending solid angle, Ω_i,

$$\sigma_t(\Omega_i, P) = \sigma_t(P) - \int_0^{\Omega_i} \frac{d\sigma}{d\Omega} d\Omega, \qquad (4.14)$$

where $d\sigma/d\Omega$ is the effective differential cross section for detected neutral particles coming forward from the detector. The major contribution to $d\sigma/d\Omega$ is the elastic differential cross section. We approximate Eq. (4.14) by a linear function of the solid angle for the purposes of least squares fitting, i.e.,

$$\sigma_t(\Omega_i, P) = \sigma_t(P) - \alpha(P)\Omega_i \ . \qquad (4.15)$$

Adoption of this approximation is justified by visual observation of the graphs of cross section versus solid angle, by the fact that quadratic or exponential functions do not improve the fits significantly, and by estimating the contribution of nonlinear terms from the elastic differential cross section. Nonlinear contributions were always smaller than the statistical errors on individual points.

The raw values of Ω_i were determined from the geometric solid angle subtended by the individual detector conversion volumes as viewed from the center of the target. These were corrected for the finite length of the target, attenuation of the incident and scattered particles through the target, and for the drop in detector efficiency near the edges of the conversion volumes. As discussed in

Sec. III D, the last effect was measured experimentally. The raw and corrected solid angles are listed in Table I for all modules at all detector positions. The corrections were of order 10% or less. Uncertainties had negligible effect on the cross sections.

For the new data there were twelve solid angles for each momentum and target; for the old and doubly-chopped, there were eight. Since correlations among the points existed, it was necessary to write χ^2 for the fitting procedure as

$$\chi^2 = \sum_{i,j} [\sigma_t(\Omega_i, P) - \sigma_t(P) + \alpha(P)\Omega_i] E_{ij}^{-1} \times [\sigma_t(\Omega_j, P) - \sigma_t(P) + \alpha(P)\Omega_j] . \quad (4.16)$$

The error matrix, E_{ij}, was determined from the variances in the following way: The diagonal elements were the sums of the average variances, $V_t^d(\Omega, P)$ $V_t^a(\Omega, P)$, and V_t^m appropriate to the given solid angle. The off-diagonal terms connecting a given module at different positions were set equal to $V_t^a(\Omega, P)$. The off-diagonal terms connecting different modules at the same detector position were set equal to V_t^m.

For each momentum bin and target, χ^2 was minimized with respect to the parameters $\sigma_t(P)$ and $\alpha(P)$. The values of $\alpha(P)$ were not well determined, but were consistent with a smooth momentum dependence. The results of this first stage are shown in Fig. 8. In the second stage of the fitting, the values indicated by the smooth curve were used to fix the parameters, $\alpha(P)$, and only $\sigma_t(P)$ were allowed to vary. The resultant values of χ^2 were not significantly different between the two stages. Two examples of the extrapolation are shown in Fig. 9. The variances $V_t^d(P)$, $V_t^a(P)$, and V_t^m were determined from the parameter variance matrix in the same spirit as in the previous section.

Summing the individual values of χ^2 over momentum bins and the two targets for the old data, we obtained $\sum \chi^2 = 432$ for 308 DF. For the new data, this was 490 for 484 DF, and for doubly chopped data it was 305 for 364 DF. The over-all distribution of $P(\chi^2)$ for the 140 fits was fairly flat. Only three fits had $P(\chi^2) < 0.01$, and another 19 had $P(\chi^2) < 0.10$. There was no systematic concentration of the poorer fits in a particular momentum region. No correlation of bad fits at the same momentum between hydrogen and deuterium targets was found. The only tendency was for the poorer fits to concentrate in the old data and the better fits to concentrate in the doubly chopped data. No weighting of the data on the basis of χ^2 was done in subsequent analysis.

5. *Combination of Data Sets*

The three data sets were compared in a search for any obvious systematic differences. In indi-

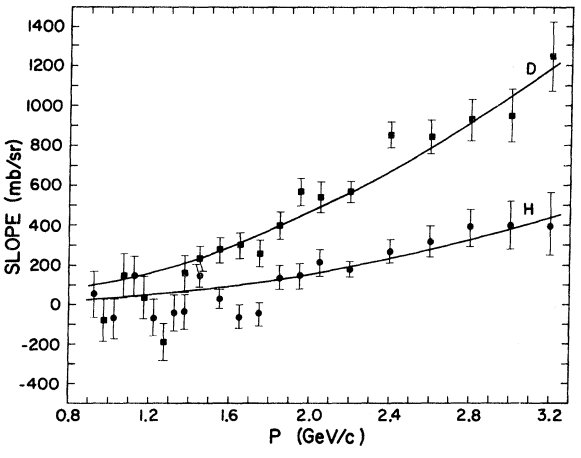

FIG. 8. Slopes for extrapolation to zero solid angle in the determination of the total cross sections. The individual points were determined during the first step. The values indicated by the lines were used in the final fits.

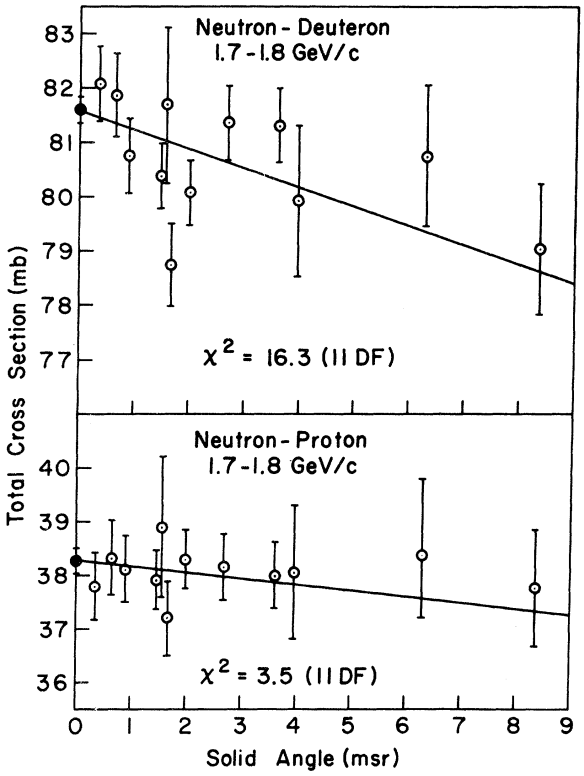

FIG. 9. Extrapolation to zero solid angle. The examples shown are from the new data, and they represent very good and very poor values of χ^2. Most fits gave values in the range $7 < \chi^2 < 15$ for 11 DF.

vidual momentum bins the differences seemed to be statistically acceptable. The 22 points in each of the data sets for hydrogen and deuterium were combined to form an average over the entire momentum range. There was a difference of about (0.2 ± 0.1) mb between the old and new results for hydrogen. Similar comparisons among all other combinations showed no significant differences. Therefore, we combined the sets on the basis of their statistical weights.

Data at all 22 momentum points from 0.9 to 3.6 GeV/c were fitted simultaneously in order to account for monitor normalization correlations. This was done separately for hydrogen and deuterium. We introduced 25 parameters, the cross sections $\sigma(P_k)$ in each of the 22 momentum bins, $k = 1, 2, \ldots, 22$, and a normalization shift N_t for each of the three data sets, $t = 1, 2, 3$. We emphasize that these latter quantities were introduced solely to account for correlations in the statistical uncertainties due to the common normalization for all momenta. The values of N_t do *not* represent systematic renormalization of our results. They were constrained to be zero within the variances permitted by monitor statistics. The individual cross sections were weighted by the combined variances due to detector and accidental statistics. Further we allowed for correlations due to timing uncertainty and for a small (5%) correlation between adjacent momentum bins which split the data from the PHA channel on the boundary. Thus,

$$\chi^2 = \sum_{k,t} \frac{[\sigma_t(P_k) - \sigma(P_k) - N_t]^2}{[V_t^d(P) + V_t^a(P)]} + \sum_t \frac{N_t^2}{V_t^m} + \sum_{t,k,l} [\sigma_t(P_k) - \sigma(P_k) - N_t] C_{kl} [\sigma_t(P_l) - \sigma(p_l) - N_t], \tag{4.17}$$

where C_{kl} accounts for the correlations and timing uncertainties.

The χ^2 values were 45 for 44 DF $[P(\chi^2) = 0.5]$ for hydrogen, and 52 for 44 DF $[P(\chi^2) = 0.2]$ for deuterium. The only value of N_t significantly different from zero was (-0.2 ± 0.1) mb for the old hydrogen data set.

In order to obtain an over-all normalization uncertainty for the experiment, we used

$$\frac{1}{V^m} = \sum_t \frac{1}{V_t^m} , \tag{4.18}$$

which yields an uncertainty of 0.05 mb for both hydrogen and deuterium.

The points in the four lowest momentum bins, derived solely from the doubly chopped data, were shifted by the appropriate values of N_t determined in this analysis: +0.08 mb for hydrogen and +0.13 mb for deuterium.

For individual data points, the uncertainties in the cross sections after averaging were taken to be the square roots of the appropriate diagonal element of the parameter error matrix. Correlations between points (aside from the monitor correlations) are about 5% for adjacent points below 2.6 GeV. Above that momentum, the uncertainties are increasingly correlated due to the uncertainties in the timing calibration. For deuterium, we estimate that the correlation coefficient between the uncertainties in the two highest momentum bins is 0.74. There is a point-by-point correlation between the hydrogen and deuterium cross sections in the same momentum bin because the same vacuum target runs were used for both calculations. The correlation coefficient is about 0.35, and it varies only weakly with momentum.

V. RESULTS

A. Total Cross Sections

Our results for neutron-proton and neutron-deuteron total cross sections are given in Fig. 10 and

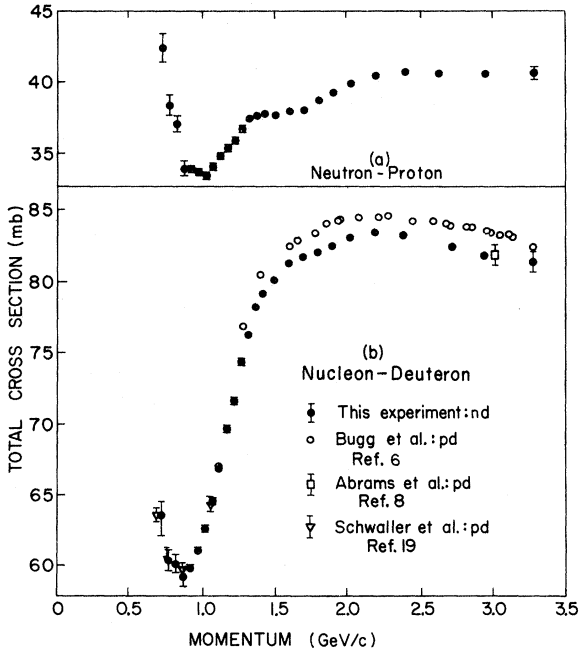

FIG. 10. (a) Neutron-proton total cross sections; (b) nucleon-deuteron total cross sections.

Table IV. The uncertainties quoted for individual momentum bins are those due to combined statistical and timing uncertainties. Systematic uncertainties based on target parameters are estimated at 0.05% for hydrogen and 0.1% for deuterium. Systematic uncertainties arising from several possible sources of beam contamination are estimated to be less than 0.07% for hydrogen and 0.10% for deuterium. These and statistical uncertainties arising from normalization are quoted separately.

B. $I=0$ Cross Sections

With previously measured values of the pp total cross section[6,7,19] and our results for the np total cross section, it is possible to compute a total cross section for the state with isospin $I=0$ from the formula

$$\sigma(I=0)=2\sigma(np)-\sigma(pp)\,. \tag{5.1}$$

It was necessary to smooth the np data below 1.0 GeV/c and to smooth the pp data below 1.4 GeV/c. The pp data were interpolated in order to evaluate

TABLE IV. Total cross sections: neutron-proton, neutron-deuteron, nucleon-nucleon ($I=0$), and neutron-neutron.

Momentum interval (GeV/c)	Average momentum (GeV/c)	Total cross sections (mb) $\sigma(np)$ [a,c]	$\sigma(nd)$ [b,c]	$\sigma(I=0)$ [d]	$\sigma(nn)$ [e]
0.70–0.75	0.725	42.80±1.02	63.55±1.02	58.1±3.0	20.2±1.1
0.75–0.80	0.775	38.63±0.72	60.73±0.75	53.0±3.0	22.1±0.7
0.80–0.85	0.825	37.32±0.60	60.46±0.65	48.8±3.0	23.3±0.8
0.85–0.90	0.875	33.97±0.57	59.33±0.62	45.5±2.0	24.9±0.5
0.90–0.95	0.925	34.09±0.26	60.14±0.28	42.9±0.5	26.6±0.3
0.95–1.00	0.975	33.90±0.24	61.30±0.25	40.6±0.7	28.9±0.2
1.00–1.05	1.025	33.57±0.24	62.78±0.25	38.8±1.2	30.2±0.3
1.05–1.10	1.075	34.16±0.24	64.71±0.24	38.1±1.2	32.2±0.3
1.10–1.15	1.125	34.94±0.24	67.03±0.25	37.3±2.1	34.8±0.3
1.15–1.20	1.175	35.47±0.23	69.88±0.24	35.4±2.1	37.3±0.3
1.20–1.25	1.225	36.04±0.23	71.87±0.23	33.0±2.1	40.0±0.3
1.25–1.30	1.275	36.85±0.22	74.64±0.24	31.2±1.1	41.9±0.3
1.30–1.35	1.325	37.60±0.22	76.30±0.23	30.5±1.1	44.5±0.3
1.35–1.40	1.375	37.85±0.22	78.28±0.23	29.8±1.1	46.2±0.4
1.40–1.45	1.425	37.98±0.21	79.17±0.22	29.4±0.4	47.3±0.3
1.45–1.55	1.500	37.82±0.16	80.27±0.16	28.5±0.3	48.1±0.3
1.55–1.65	1.600	38.12±0.16	81.46±0.17	28.7±0.3	48.4±0.3
1.65–1.75	1.700	38.21±0.16	81.76±0.17	28.8±0.3	48.2±0.3
1.75–1.85	1.800	38.85±0.16	82.19±0.17	30.2±0.3	47.9±0.3
1.85–1.95	1.900	39.35±0.17	82.60±0.18	31.3±0.3	47.9±0.3
1.95–2.10	2.022	39.99±0.15	83.14±0.16	32.7±0.3	47.9±0.3
2.10–2.30	2.193	40.50±0.14	83.41±0.15	34.0±0.3	47.7±0.3
2.30–2.50	2.391	40.67±0.16 [f]	83.28±0.18 [f]	35.2±0.3	47.1±0.3
2.50–2.80	2.627	40.75±0.17 [f]	82.52±0.21 [f]	36.0±0.4	46.2±0.3
2.80–3.20	2.944	40.76±0.25 [f]	81.87±0.37 [f]	36.9±0.5	45.0±0.4
3.20–3.60	3.277	40.83±0.46 [f]	81.43±0.70 [f]	38.0±1.0	44.0±1.0

[a] Over-all scale uncertainty due to monitor statistics = ± 0.05 mb. Estimated systematic uncertainty from all sources = ± 0.09%.

[b] Over-all scale uncertainty due to monitor statistics = ± 0.05 mb. Estimated systematic uncertainty from all sources = ± 0.16%.

[c] Estimated correlation coefficient between np and nd cross section uncertainties in the same momentum bin is 0.35.

[d] Computed from $\sigma(np)$ and previously measured proton-proton cross sections. (See Sec. V B).

[e] Computed from $\sigma(np)$ and $\sigma(nd)$ with a correction for screening effects. (See Sec. V E).

[f] Off-diagonal correlation coefficients for uncertainties in the highest four momentum bins are, in order of increasing momentum,

$$\begin{pmatrix} 0.06 & & \\ 0.08 & 0.14 & \\ 0.09 & 0.14 & 0.24 \end{pmatrix}_{\sigma(np)} \quad \text{and} \quad \begin{pmatrix} 0.26 & & \\ 0.34 & 0.55 & \\ 0.35 & 0.57 & 0.74 \end{pmatrix}_{\sigma(nd)}$$

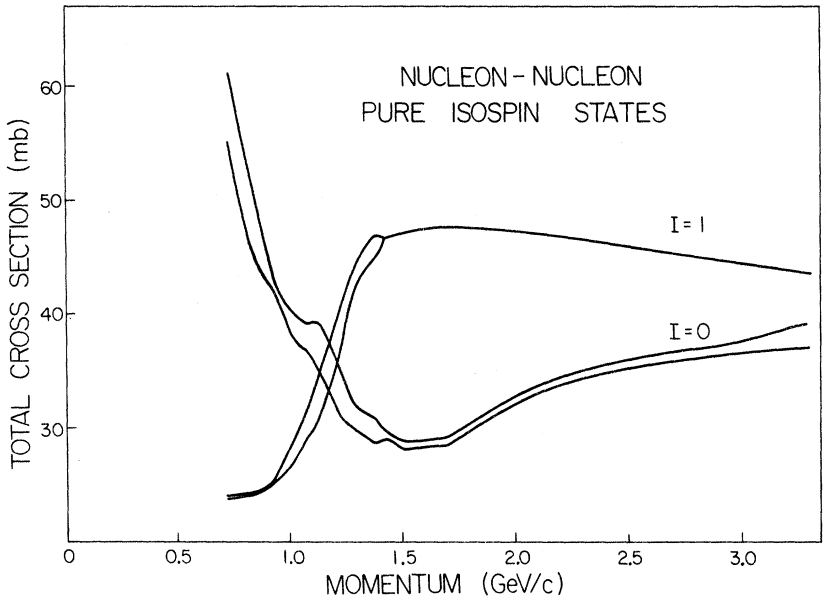

FIG. 11. Nucleon-nucleon total cross section in the $I=0$ and $I=1$ states. Points were computed from our measured np total cross sections and various measurements of pp total cross sections (Refs. 6, 7, and 19).

the cross sections at our momenta. The results are shown in Table IV and Fig. 11. Considerable uncertainty arises from inconsistency among the various measurements of pp cross sections between 1.0 and 1.4 GeV/c. The uncertainties on the tabulated points and the error corridors on the graph include these effects.

C. Comparison of pd and nd Total Cross Sections

Our nd total cross sections agree quite well with the pd results of Abrams *et al.*[8] at 3.0 GeV/c and Schwaller *et al.*[19] below 1.2 GeV/c. If one accepts the quoted uncertainties, the principle of charge symmetry is confirmed to 0.8% at ~1.0 GeV/c and 0.5% at 3 GeV/c.

There is, however, a constant ~1.5 mb difference between our data and the pd cross sections of Bugg *et al.*[6] The shapes are almost identical as functions of momentum. The 1.5-mb difference between the data of Bugg *et al.* and the result of Abrams *et al.* was discussed and partially resolved by Riley.[15] There remained an unexplained difference of 1.17 mb at 3 GeV/c. We find that a subtraction of 1.5 mb from the data listed in Ref. 6 makes it fully compatible with our results, with those of Refs. 8 and 19, and also with those of Galbraith *et al.*[20] at 8 GeV/c.

Until unanimity is established in the various pd results, a violation of charge symmetry up to 2% is not ruled out by these data. However, we are strongly inclined toward the conclusion that charge symmetry is satisfied to 0.5% and Ref. 6 has large systematic errors.

D. Structure

We see no evidence of resonant structure in either the $I=0$ or $I=1$ cross sections. The bump in the np cross section at about 1.4 GeV/c seems to be explained entirely by the minimum in the $I=0$ cross section and the knee of the plateau in the $I=1$ cross section. It is probably not caused by the so-called $D^*(2190)$ bump[21] observed in πd scattering and in the reaction $np \to \pi d$.[22] The cross section for the latter reaction is of order 1.5 mb. We have subtracted it from our total cross section results and find only small changes in shape, predominantly at momenta lower than the 1.4 GeV/c bump.

E. The Neutron-Neutron Cross Section

Values for the n-n cross section may be obtained from our data as the differences between $\sigma(nd)$ and $\sigma(np)$. (See Table IV.) A correction for screening effects is required but due to several factors, cannot be calculated with certainty.

The approximate calculation which has been made is described below. The cross section defect is defined by the equation

$$\sigma(nn) = \sigma(nd) - \sigma(np) - \delta\sigma . \tag{5.2}$$

For this paper we use the form given by Franco and Glauber[23] and add the charge-exchange term of Wilkin,[24]

$$\delta\sigma = \frac{1}{4\pi}\{2\sigma(np)\sigma(nn)(1-\alpha(np)\alpha(nn)) - \tfrac{1}{2}[\sigma^2(nn)(1-\alpha^2(nn)) - \sigma^2(np)(1-\alpha^2(np))]\}\frac{1}{2\pi}\int [S(q)e^{-\beta^2 q^2}]d^2q\,, \tag{5.3}$$

where α is the ratio of real to imaginary parts of the forward scattering amplitude, $S(q)$ is the form factor of the deuteron, and β is the slope of the NN amplitude. In calculating the charge exchange term we assume $\sigma(nn)=\sigma(pp)$.

The values of $\alpha(nn)$ are assumed to be equal to $\alpha(pp)$ calculated by Söding.[25] The values for $\alpha(np)$ are taken from Carter and Bugg.[26] The form assumes $\beta(np)=\beta(pp)$, but values of β are obtained by using $\beta=\frac{1}{2}[\beta(np)+\beta(pp)]$ obtained from a compilation of NN data.[27]

The deuteron wave function is a repulsive core form[28] and includes only S wave. The $\sigma(np)$ and $\sigma(nn)$ cross sections are averaged over Fermi motion in the deuteron, and the flux correction has been applied.[29]

The discrepancy between calculated $\sigma(nn)$ and measured $\sigma(pp)$ can easily be attributed to systematic uncertainties in the screening correction. Values of α are not known well, spin-dependent corrections[30] have not been included, and changing deuteron wave functions can alter the values by ±1 mb.

ACKNOWLEDGMENTS

We are grateful to Professor Milton White, Professor Walter Wales, and the staff of the Princeton-Pennsylvania Accelerator for their support of this work. Special thanks are due Robert Jankowicz for designing and building a target system which met a number of demanding specifications. We thank Carl Meuhleisen for constructing the neutron detector. Much of the analysis was done with the computer facilities of the Rutgers Bubble Chamber Group, funded under NSF Grants No. GU 1592 and GP 29084.

*Work supported in part by the National Science Foundation under Grants No. NSF GU-1592, GP-14703 and GP-34699, and by the U. S. Atomic Energy Commission under Contract No. AT (11-1)-3072 [formerly AT(30-1)-2137].

†Present address: Liverpool Group, Daresbury Nuclear Physics Laboratory, Daresbury, New Warrington Lanes, England.

‡Present address: General Electric Research and Development Center, Room 4C40, P. O. Box 8, Schenectady, New York 12301.

§Present address: MP Division, Los Alamos Scientific Laboratory, Los Alamos, New Mexico 87544.

‖Present address: Donner Laboratory, University of California, Berkeley, California.

[1]R. E. Mischke, T. J. Devlin, W. Johnson, J. Norem, K. Vosburgh, and W. Schimmerling, Phys. Rev. Lett. 25, 1724 (1970).

[2]H. Palevsky, J. L. Friedes, R. J. Sutter, R. E. Chrien, and H. R. Muether, in *Proceedings of the International Congress on Nuclear Physics, Paris, 1964,* edited by P. Gugenberger (Centre National de la Recherche Scientifique, Paris, France, 1964), p. 162.

[3]Y. M. Kazarinov and Y. N. Simonov, Zh. Eksp. Teor. Fiz. 43, 35 (1962) [Sov. Phys.–JETP 16, 24 (1963)].

[4]V. P. Dzhelepov, B. M. Golovin, Y. M. Kazarinov, and N. N. Semenov, in *Proceedings of the CERN Symposium on High-Energy Accelerators and Pion Physics, Geneva, 1956* (European Organization of Nuclear Research, Geneva, 1956), Vol. 2, p. 115.

[5]A number of measurements at higher energies have been made. J. H. Atkinson, W. N. Hess, V. Perez-Mendez, and R. Wallace, Phys. Rev. 123, 1850 (1961); V. S. Pantuev, M. N. Khachaturyan, and I. V. Chuvilo, Yad. Fiz. 1, 134 (1965) [Sov. J. Nucl. Phys. 1, 93 (1965)]; E. F. Parker, H. R. Gustafson, L. W. Jones, M. J. Longo, P. V. Ramana Murthy, F. E. Ringia, and B. Cork, Phys. Lett. 31B, 246 (1970); M. N. Kreisler, L. W. Jones, M. J. Longo, and J. R. O'Fallon, Phys. Rev. Lett. 20, 468 (1968); L. Ozhdyani, V. S. Pantuyev, M. N. Khachaturyan, and I. V. Chuvilo, Zh. Eksp. Teor. Fiz. 42, 392 (1962) [Sov. Phys.–JETP 15, 272 (1962)]; J. Engler, K. Horn, J. König, F. Mönnig, P. Schludecker, H. Schopper, P. Sievers, H. Ullrich, and K. K. Runge, Phys. Lett. 27B, 599 (1968).

[6]D. V. Bugg, D. C. Salter, G. H. Stafford, R. F. George, K. F. Riley, and R. J. Tapper, Phys. Rev. 146, 980 (1966).

[7]V. P. Dzhelepov, S. V. Moskalev, and S. V. Medred, Dokl. Adad. Nauk SSSR 104, 380 (1955); O. Chamberlain, G. Pettergill, E. Segrè, and C. Weigand, Phys. Rev. 93, 1424 (1954); O. Chamberlain, E. Segrè, and C. Weigand, *ibid.* 81, 284 (1951); J. R. Holt, J. C. Kluyver, and J. A. Moore, Proc. Phys. Soc. Lond. 71, 781 (1958).

[8]R. J. Abrams, R. L. Cool, G. Giacomelli, T. F. Kycia, B. A. Leontić, K. K. Li, and D. N. Michael, Phys. Rev. D 1, 2477 (1970).

[9]R. J. Glauber, Phys. Rev. 100, 242 (1955).

[10]W. E. Cleland, D. Freytag, B. Goz, T. J. Devlin, R. Esterling, and K. Vosburgh (unpublished).

[11]T. J. Devlin, P. F. Shepard, J. Solomon, E. F. Beall, and G. Sayer, Phys. Rev. Lett. 18, 54 (1967); G. A. Sayer, E. F. Beall, T. J. Devlin, P. F. Shepard, and J. Solomon, Phys. Rev. 169, 1045 (1968).

[12]R. E. Mischke, P. F. Shepard, and T. J. Devlin, Phys. Rev. Lett. 23, 542 (1969).

[13]K. Vosburgh, T. J. Devlin, R. Esterling, B. Goz, D. A. Bryman, and W. E. Cleland, Phys. Rev. D 6, 1834 (1972).
[14]W. Schimmerling, T. J. Devlin, W. Johnson, K. G. Vosburgh, and R. E. Mischke, Phys. Rev. C 7, 248 (1973).
[15]K. F. Riley, Phys. Rev. D 1, 2481 (1970).
[16]R. J. Tapper, Rutherford Laboratory Report No. NIRL/R/95, 1965 (unpublished).
[17]W. J. Hogan, A. J. S. Smith and P. A. Piroué, Phys. Rev. 166, 1472 (1968).
[18]Particle Data Group, Phys. Lett. 39B, 1 (1972).
[19]P. Schwaller, B. Favier, D. F. Measday, M. Pepin, P. U. Renberg, and C. Serre, CERN Report No. CERN 72-13, 1972 (unpublished).
[20]W. Galbraith, E. W. Jenkins, T. F. Kycia, B. A. Leontić, R. H. Phillips, A. L. Read, and R. Rubenstein, Phys. Rev. 138, B913 (1965).
[21]S. Mandelstam, Proc. R. Soc. Lond. A244, 491 (1958).
[22]D. F. Bartlett, C. E. Friedberg, K. Goulianos, I. S. Hammerman, and D. P. Hutchinson, Phys. Rev. D 1, 1984 (1970).
[23]V. Franco and R. J. Glauber, Phys. Rev. 142, 1195 (1966).
[24]C. Wilkin, Phys. Rev. Lett. 17, 561 (1966).
[25]P. Söding, Phys. Lett. 8, 285 (1964).
[26]A. A. Carter and D. V. Bugg, Phys. Lett. 20, 203 (1966).
[27]Particle Data Group, LBL Report No. UCRL-20000*NN* (unpublished).
[28]L. Durand III, Phys. Rev. 123, 1393 (1961).
[29]G. Fäldt and T. E. O. Ericson, Nucl. Phys. B8, 1 (1968).
[30]G. Alberi and M. A. Gregorio, Nuovo Cimento Lett. 5, 585 (1972).